Medicine in Novel Technology and Devices 18 (2023) 100240

Contents lists available at ScienceDirect

Medicine in Novel Technology and Devices

journal homepage: www.journals.elsevier.com/medicine-in-novel-technology-and-devices/

Swirling flow and capillary diameter effect on the performance of an active dry powder inhalers

Mohammad Hasan Taheri [a], Nematollah Askari [a], Yaning Feng [b], Malikeh Nabaei [c], Mohammad S. Islam [d], Ali Farnoud [e], Xinguang Cui [b,*]

[a] Department of Mechanical Engineering, Faculty of Imam Khomeini, Behshahr Branch, Technical and Vocational University (TVU), Mazandaran, Iran
[b] School of Aerospace Engineering, Huazhong University of Science and Technology, Wuhan, China
[c] Faculty of Biomedical Engineering, Amirkabir University of Technology (Tehran Polytechnic), Tehran, Iran
[d] School of Mechanical and Mechatronic Engineering, University of Technology Sydney (UTS), 15 Broadway, Ultimo, NSW, 2007, Australia
[e] Computational Health Center, Helmholtz Munich, Munich, Germany

ARTICLE INFO

Keywords:
Computational fluid dynamics
Dry powder inhalers
Swirling flow

ABSTRACT

For patients with lung disease, dry powder inhalers (DPI) are profoundly beneficial. The current study introduces and develops a series of dry powder inhalers (DPIs). A capsule-based (size 0) active DPI was considered. The study aims to investigate whether swirling flow and outlet capillary diameter (d_{c_out}) affect the percentage of emitted doses (ED) released from the capsule. Spiral vanes were added to the capillary inlet to produce a swirling flow. Computational fluid dynamics (CFD) was applied to simulate the problem. The results were compared with previous in vitro and numerical studies to validate the results. Based on the derived results, the small swirl parameter (SP) enhances the secondary flow and recirculation zone. It increases the central jet flow, which increases the ED value by about 5–20% compared to no-swirl flow. However, as the airflow rate increases, the recirculation zone enlarges, vorticities become dominant, and asymmetrical flow patterns emerge. Consequently, ED % drops significantly (more than 50%). As d_{c_out} decreases, the vorticities around the outlet capillary become more potent, which is undesirable. Indeed, the emptying of the capsule does not happen ideally. The research provides a perspective on the device's design and DPI performance.

1. Introduction

Dry powder inhalers (DPIs) have been used to efficiently administrate medications and aerosols. For many years, an increasing number of inhalation devices have been developed. However, the ideal device would be efficient, reproducible, precise, stable, comfortable, versatile, environmentally compatible, and affordable [1]. DPIs are a drug delivery method used to treat various lung diseases. DPIs have distinct advantages that make them suitable for small and large molecules [2]. DPIs can deliver high-dose inhaled medications quickly and efficiently. As DPIs become increasingly popular for treating pulmonary disease patients, they simplify the inhalation technique, provide reproducible doses, and improve adherence to aerosol therapy among patients.

Several DPI-related mainstream developments can be outlined. The following are the top five [3].

(1) to improve the design of previous inhaler configurations.
(2) to improve and modify drug formulation, also known as particle engineering.
(3) to produce the formulation and design of inhalers for vaccines and systemically acting drugs.
(4) to comprehend and control drug distribution and deposition in the lungs via DPIs.
(5) a variety of other innovative developments.

This study follows the first mainstream and examines whether swirling flow impacts the design of medical devices in a positive or negative manner.

Airflow rate, formulation, and device design are the three main factors that affect the efficiency of DPIs [4]. In DPIs with dry powder formulations, the main force to overcome the inter-particle force through inhalation is airflow. As the powder does not require much energy to aerosolize, increasing the inhalation flow rate increases the system's energy and improves dispersion [4]. DPIs use one of two formulations:

* Corresponding author.
E-mail address: xinguang_cui@hust.edu.cn (X. Cui).

https://doi.org/10.1016/j.medntd.2023.100240
Received 13 January 2023; Received in revised form 4 May 2023; Accepted 14 May 2023

fine powder drug blended with larger carrier particles or the drug alone. If the deep lung is the target, the drug particle diameter should be between 1 and 5 μm. Particles of 1–2 μm are best suited for reaching the small airways and alveolar epithelium [5]. Device design is another crucial parameter that influences DPI performance. Geometry has a significant effect on airflow dynamics, resistance, drag forces, and impaction patterns, and even minor changes in the geometry of DPIs can significantly affect their performance [4,6].

There are many benefits to DPIs, including rapid delivery of high-dose inhaled medications. However, many children are not prescribed DPIs due to a low lung delivery efficiency and the complexity of the device. An inline dry powder inhaler (DPI) uses an external gas source like a ventilation bag, an air-filled syringe, or compressed air instead of traditional inhalation driven DPIs. An essential benefit of this approach is the ability to control and reproduce actuation air volumes and flow rates with little variability. Children and infants who cannot operate passive DPIs may benefit from inline devices that require external air for actuation. Also, these devices may help administer powder-based aerosols to subjects with compromised lung function or if they are involved in noninvasive ventilation via masks, nasal prongs, or conventional ventilation via endotracheal tubes [6–9].

Active DPIs operating at low air actuation volumes have caught the attention of researchers. A DPI of this sort is widely used for infants and children whose air volume is insufficient to stimulate the device. Aerosol administration is also tested with active DPIs in animal studies [10–13].

Longest and Farkas have done plenty of research on low-air volume DPIs [14–24]. They looked into capsule-based DPIs in which airflow flows through an orifice with a high momentum air jet. Their research revealed that the inlet and outlet orifices should be designed so that their axes are aligned. Furthermore, the inlet airflow jet should not directly impinge on the aerosol powder bed, and the secondary flow velocity should initiate aerosol dispersion.

Longest et al. [17] presented a computational fluid dynamics (CFD) study on different DPI designs as the most recent study on this topic. They examined various inlet and outlet orifice diameters and compared their outcomes to previous experimental studies. They noticed that the CFD prediction is very close to the best device experiment study that has been published.

Furthermore, Ahookhosh et al. [9] experimented with DPI and Metered-Dose Inhaler (MDI) performance. They set out to examine how they perform with the deposition parameters in a realistic human airway. They found that MDI delivered more drugs than DPI. They also carried out a CFD study to address the limitations of their previous study [25]. As presented in a recent publication, Ahookhosh et al. [26] examined the optimization of a Pressurized Metered Dose Inhaler (pMDI) in a human airway model. CFD simulations were used to analyze flow structure inside pMDI and particle deposition. According to the study, there is a strong dependence on inhalation flow rate and inhaler geometry.

Dai et al. [27] investigated the devices' effectiveness in their numerical study on active DPIs. In their numerical study on active DPIs. Their primary objective was to analyze the effects of inlet flow rate and piercing aperture location on device-emptying. Their findings demonstrate the noticeable effect of these parameters.

Recent studies have examined how swirling flow can be utilized to improve drug delivery into targeted areas. Gurumurthy and Kleinstreuer [28] published a study investigating MDIs and improving oral drug delivery to specific target areas, particularly deeper lung regions. Various helical stream inhalation modes were used, each of which produced different swirl numbers. They found that a suitable swirl number significantly increased drug delivery. The work by Last et al. [29] presented an applied micro-swirl nozzle for the delivery of drugs to the lungs. Alfano et al. [30] investigated swirl-based dry powder inhalers using CFD-DEM simulation. Further, Sommerfeld [31] numerically evaluated swirl-type inhalers.

A swirl-based DPI significantly aids in the deaggregation of active pharmaceutical ingredients (APIs) according to the above research. In addition, swirling jets could counter gravity and reduce axial momentum.

This study's motivation is to develop a dry powder inhaler (DPI) platform to deliver inhaled therapeutic medications to the lungs through aerosolization of excipient enhanced growth (EEG) and other spray-dried powders. As a part of this study, the developed device is intended for traditional oral inhalation in adults, and inline aerosol administration in adults and children. Therefore, a capsule-based DPI for oral inhalation based on a CFD approach is developed. As a novelty, new DPI designs are defined and analyzed for each case with swirling flow at the inlet and outlet capillaries of different diameters. Another study goal is to examine how these parameters affect device emptying.

2. Design and numerical simulations

2.1. DPI design

This study includes multiple new, inline DPI. According to previous studies [17,22], a capsule-based drug loading design with an inlet capillary, outlet capillary, and containment volume (capsule of size 0: capacity = 0.68 mL, cap-length = 18 mm, cap-diameter = 7.5 mm) was chosen and modeled (Fig. 1).

The low-air-volume flows from the inlet capillary into the containment based on these prior studies [17,22]. The inlet air does not pass through the powder bed directly because the aerosols are loaded on a powder bed in a containment unit. The jet airflow exits the inlet capillary, creating visible turbulence and secondary flows that cause the aerosols to disperse inside the capsule.

According to earlier studies, the inlet and outlet capillaries have a protrusion of 2 mm, which is shown in Fig. 1. Previous studies [17,22] have shown that the inlet orifice diameter should be 0.6 mm or greater.

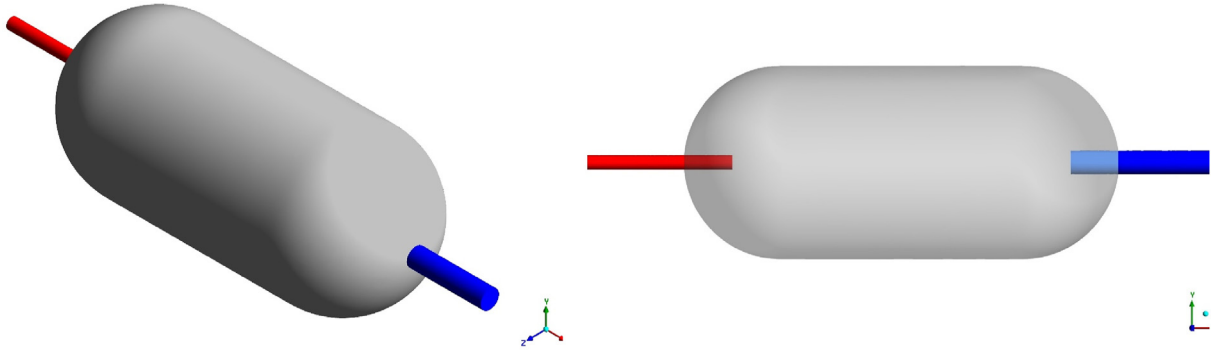

Fig. 1. A schematic of capsule -based DPI (red = inlet capillary, and blue = outlet capillary) (a) Inlet capillary with different SP (b) Outlet capillary with different diameters

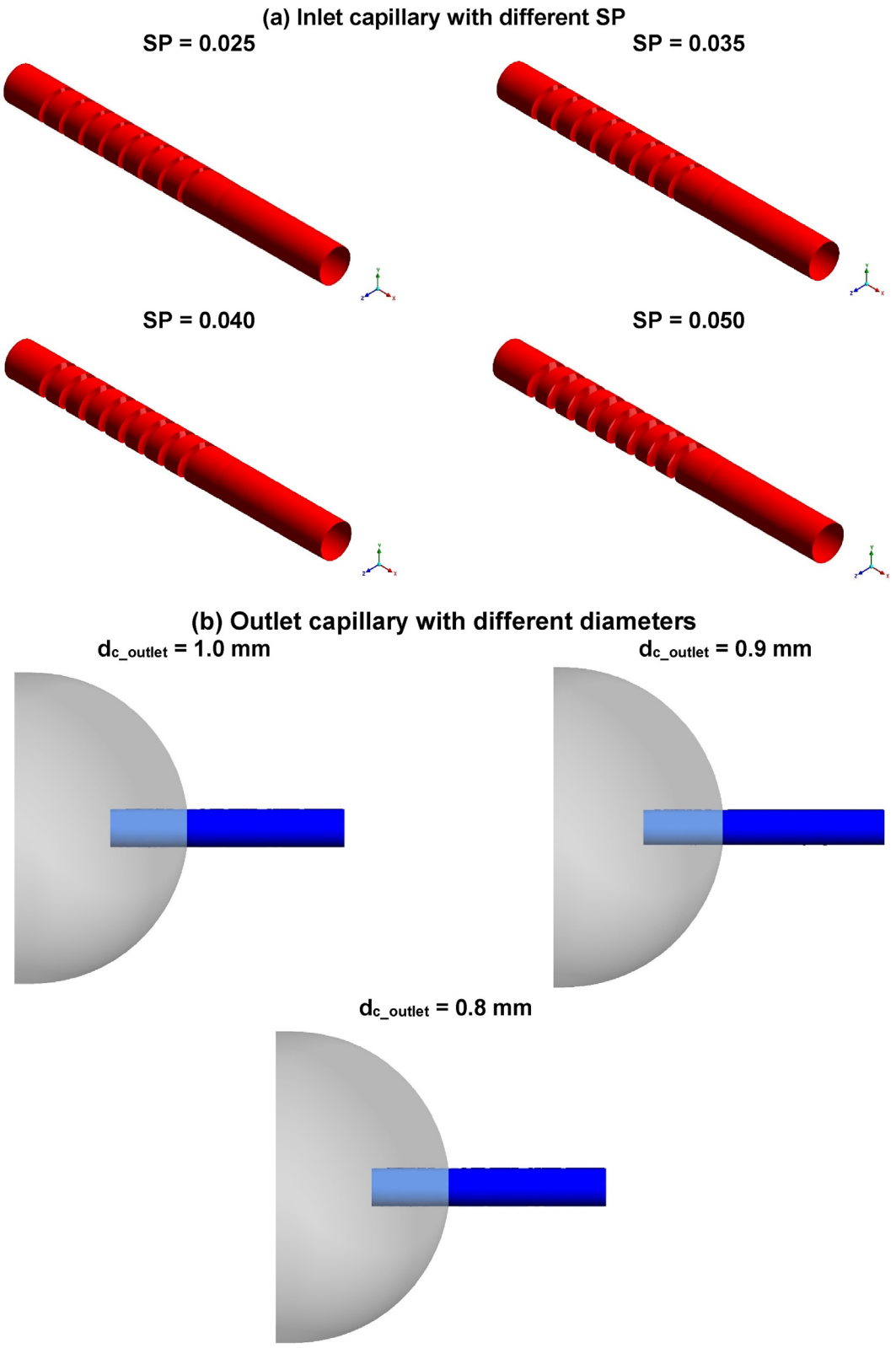

Fig. 2. Various designs in the present study; (a) for various spiral parameter (SP), (b) for various outlet capillary diameter (d_{c_outlet}).

This study set the inlet capillary diameter (d_{c_inlet}) at 0.6 mm.

In this study, a series of new devices are designed and modeled using swirling flow at the inlet capillary and different outlet capillary diameters (d_{c_outlet}). Spiral vanes were positioned on the inlet capillary unit to generate a swirling flow. Different spiral depths (SD) were applied to the inlet capillary to examine the impact of swirling flow. The swirl parameter (SP) is described as follows [32]:

$$SP = \frac{SD}{SH} \tag{1}$$

Table 1
Various scenarios implemented in the present study.

d_{c_inlet} (mm)	d_{c_outlet} (mm)	SH (mm)	SD (mm)	SP	Airflow rate (LPM)
0.6	0.8	3	0.08	0.025	3
	0.9		0.10	0.035	4
	1.0		0.12	0.040	5
			0.15	0.050	

where SH is the spiral height, and spiral pitch and SH were considered constants in this study.

Different designs and scenarios were defined using various SP and d_{c_outlet} as shown and tabulated in Fig. 2 and Table 1, respectively.

2.2. CFD simulations

A sufficient momentum has been provided by using a 10 mL syringe. The inlet airflow rates were considered 3, 4, and 5 LPM. According to the diameter of the inlet and the airflow at the inlet, the Reynolds number is greater than 6700, while the Mach number is greater than 0.5. Therefore, the airflow in the study is turbulent and compressible. It was important for the authors to select a turbulence model that was both accurate and efficient to achieve the desired results. Based on the previous research [15,17,22,27], the Low-Reynolds-Number (LRN) k-ω model is the suitable choice to model this kind of problem. The simulation was performed by using Ansys Fluent 2021 R2. Also, the simulation of the problem is time dependent. In the active DPIs, the whole process occurred in less than 0.2 s. So, the entire period of the problem is taken 0.2 s. The timestep splits into two points to decline the CPU time. In the first point, selected at 0.01 s, the timestep size and steps were set at 0.0001 s and 100, respectively. The smaller timestep was considered in the first point due to capturing the oscillatory flow and startup effect. For the rest of the period, the timestep size was selected as 0.001 s.

For the discretization, the Green-Gauss node based was selected for the gradient. Also, the second-order upwind and central difference methods were applied for the convective and diffusion terms. The second-order implicit discretization is also used for the transient term. Moreover, the Courant number was considered to be 3.

If necessary, published literature can be found on the governing equations of this model in detail [33–36]. However, the general equations of the k-ω model are presented in the following [17,27].

- turbulent kinetic energy (k):

$$k = \frac{1}{2}\left(\overline{\hat{u}^2} + \overline{\hat{v}^2} + \overline{\hat{w}^2}\right) \tag{2}$$

- specific dissipation rate (ω):

$$\omega = \frac{k^{1/2}}{S_\mu^{1/4}\hat{l}} \tag{3}$$

where $\hat{u}, \hat{v}, \hat{w}$ denote the fluctuating velocity components and as a time-average velocity. S_μ is a constant and $\hat{l}$ represents the turbulence length scale.

The behavior of turbulent fluids is comparable to molecular kinematic viscosity due to their enhanced diffusive (or dispersive) effects on momentum. To capture this analogy, the turbulent kinematic viscosity can be described as follows:

$$\hat{v}_T = \frac{k}{\omega} \tag{4}$$

As a result of the product of k and ω, and their combination, we can see that k has an increased importance related to turbulent length scale l, as follows:

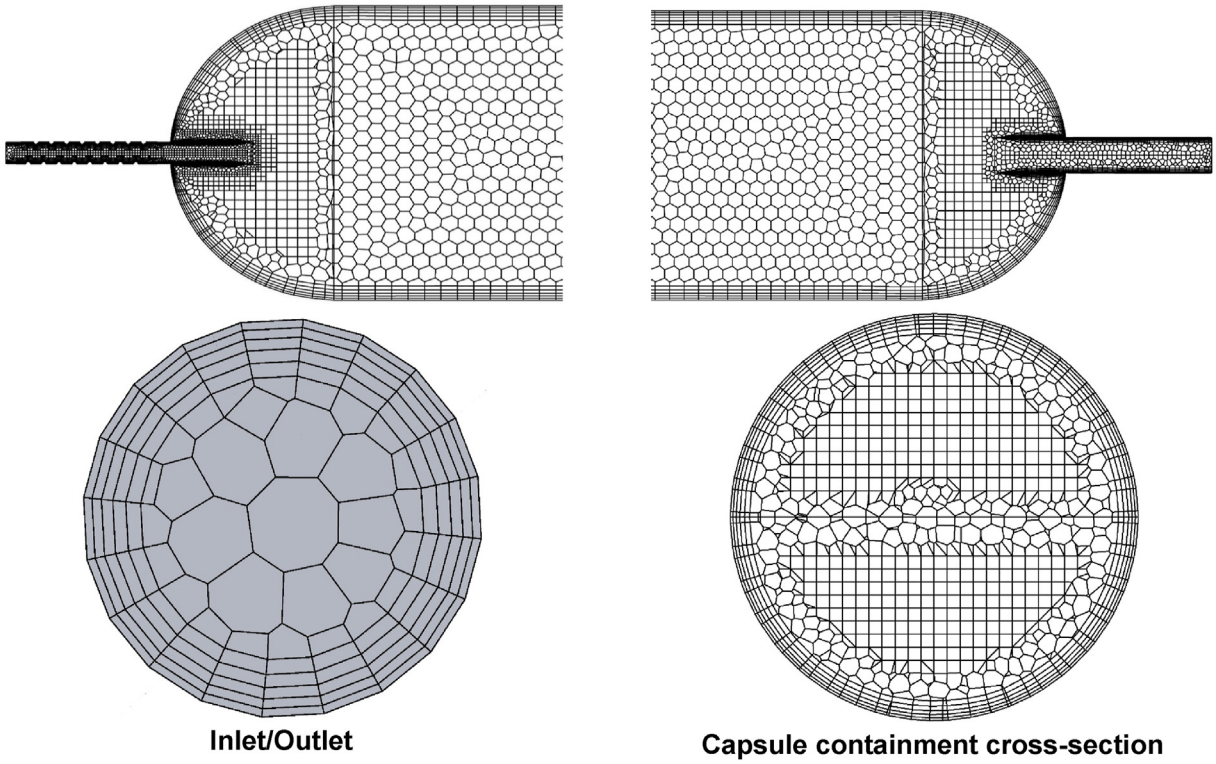

Fig. 3. View of the mesh used for the model in various cross-sections (It should be noted that a coarser mesh is presented for drawing for readers' convenience, but a finer mesh was used for solving the problem).

Table 2
Validation of the present results with previous published research.

d_{c_inlet} (mm)	d_{c_outlet} (mm)	Airflow rate (LPM)	ED (%)		
			Longest [17, 18]	Dai [27]	Present study
0.6	1.17	3	45	44.9	48.6
		4	77.2	78.0	79.3
		5	87.6	82.0	86.4

$$\widehat{k}\ \omega = \frac{k^{3/2}}{S_{\mu}^{1/4}\widehat{l}} \tag{5}$$

2.3. Meshing

In this study, a poly-hexcore scheme to generate meshes (Fig. 3) is used. In the poly-hexcore meshing, the polyhedral elements operate in the transition zone with a hexahedral element core, providing the optimal combination of mesh elements. Compared with a hexahedral or polyhedral core mesh of the same accuracy, poly-hexcore meshes reduced solve time by 20–50%. The independence of mesh from the grid was checked for velocity in all cases and scenarios. The results were independent of meshing for grids containing 1,250,000–1,500,000 cells (less than a 3% difference was observed). Also, to capture better the near wall impact on flow, five boundary layers mesh was considered to ensure the y^+ value less than one. Additionally, the mesh has a skewness of 1.3×10^{-10}.

2.4. Particle tracking

To track the particle trajectory, Discrete Phase Model (DPM) was applied using Ansys Fluent 2021 R2. Constant diameter particles ($d_{particle} = 2$ μm) with a constant density equal to 1000 (kg/m^3) were selected and initially distributed on a powder bed. Since the volume fraction of the secondary phase is less than 10^{-06}, the one-way coupled Lagrangian approach was employed to track particle trajectories. Two forces were considered to act on the particles, drag and gravity forces. The governing equation on particle motion was presented elaborately in the previous publications [15,27,37,38]. The common equation introduced in DPM and a Lagrangian frame of reference is as follows [37,38]:

$$\frac{dV_{particle}}{dt} = F_{drag}\left(V_{fluid} - V_{particle}\right) + \frac{g\left(\rho_{particle} - \rho_{fluid}\right)}{\rho_{particle}} \tag{6}$$

where the left-hand side term is particle inertia, F_{drag} denotes the particle drag force per unit particle mass, and the second term on the right-hand side represents the particle buoyancy force.

A powder bed along the bottom wall of the capsule was created.

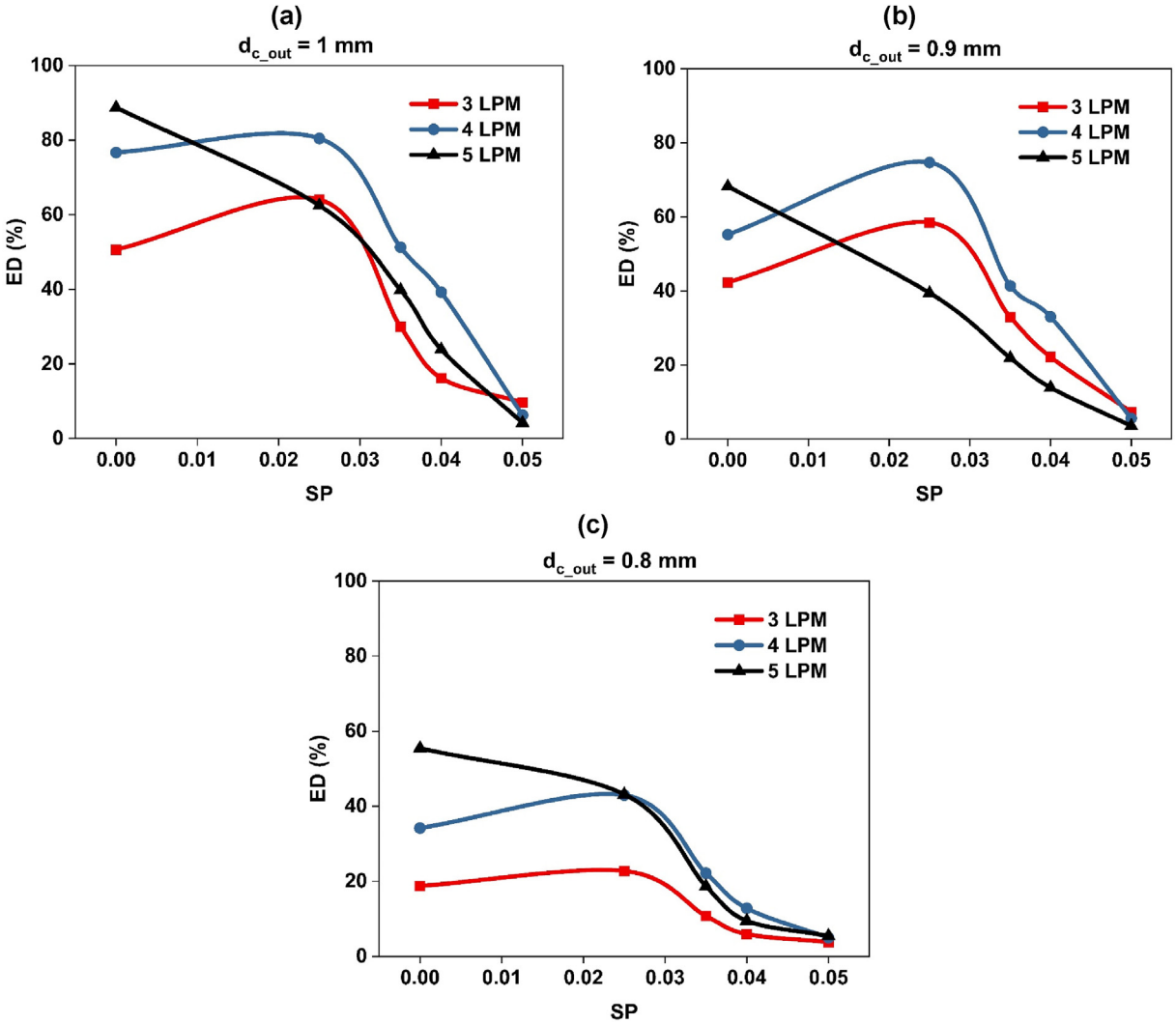

Fig. 4. Effects of airflow rate and SP on ED for (a) d_{c_out} = 1.0 mm, (b) d_{c_out} = 0.9 mm, and (c) d_{c_out} = 0.8 mm (t = 0.2 s).

Various particles number were considered to reach the independency of particles number. It was observed that for particles numbering more than 15,000, the results become independent of particle number.

3. Validation

Since there is no published research using the spiral vane on their model, to validate our outcomes, a DPI model based on the previous study presented by Longest et al. [17] (concurrent in vitro and CFD simulation) and Dai et al. [27] (CFD simulation) is generated without considering swirling flow. In their model, the inlet and orifice diameters are 0.6- and 1.17-mm. Aerosol performance was evaluated based on emitted dose (ED) percentage. ED refers to the ratio between the remaining dose and the drug's loaded dose. Comparing our model outcomes with their reported results (Table 2) showed that our generated model is reliable.

Table 3
The quantity view of ED % for different LPMs, d_{c_out}, and SPs.

SP	3 LPM			4 LPM			5 LPM		
	d_{c_out}								
	1.0 mm	0.9 mm	0.8 mm	1.0 mm	0.9 mm	0.8 mm	1.0 mm	0.9 mm	0.8 mm
	ED %								
0.000	50.61	42.31	18.75	76.68	56.27	34.18	88.7	66.23	55.45
0.025	64.06	58.45	22.74	80.45	78.62	42.96	62.5	41.66	43.16
0.035	41.91	35.89	10.74	51.27	42.68	22.18	39.8	21.38	18.68
0.040	26.22	24.16	5.93	39.24	32.12	12.81	23.9	15.98	9.47
0.050	9.66	11.31	3.82	6.27	9.35	4.96	4.2	7.59	5.45

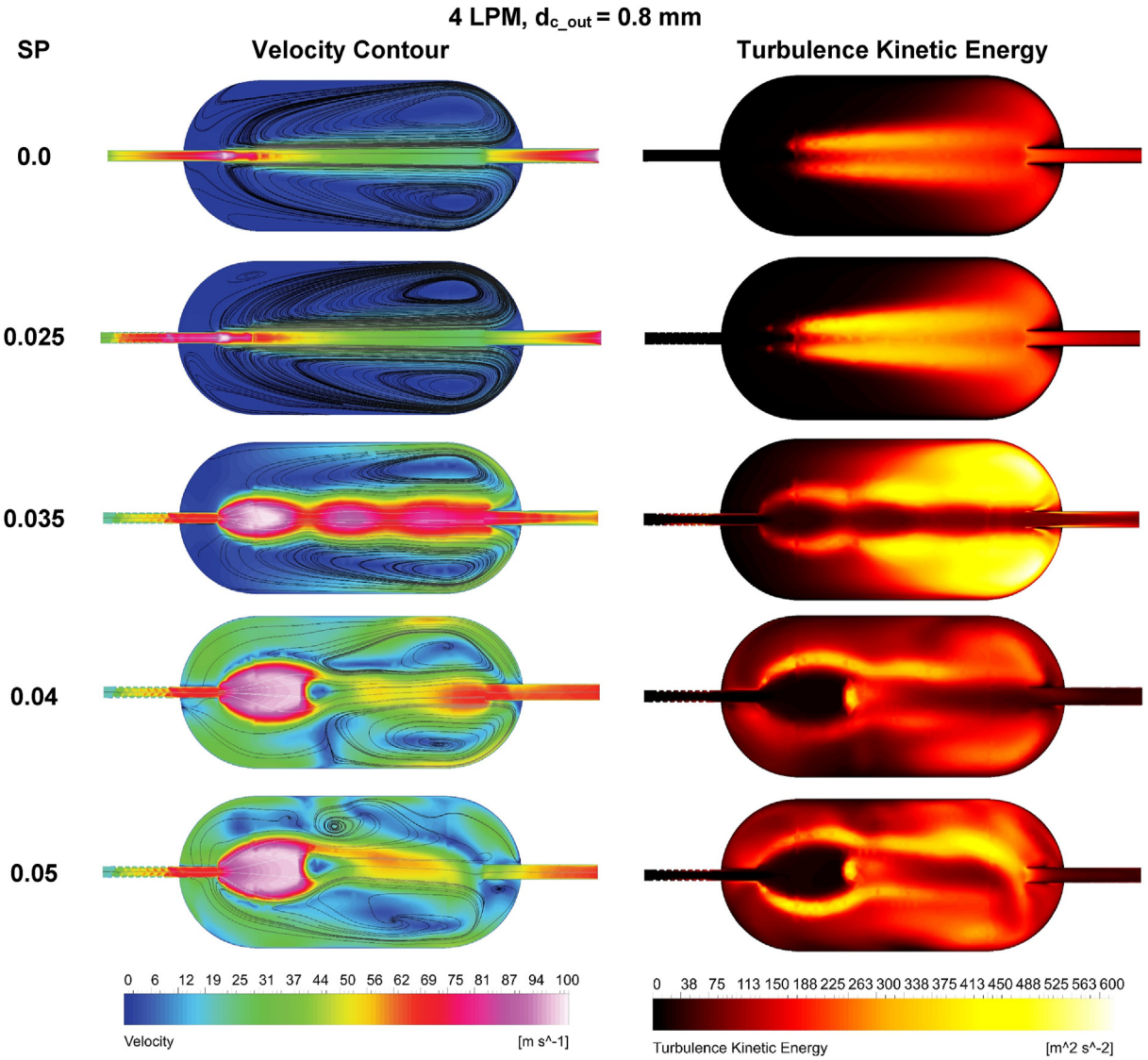

Fig. 5. Contour of velocity and turbulence kinetic energy of various SP for d_{c_out} = 0.8 mm and 4 LPM flow rate (t = 0.2 s).

4. Results

An analysis of swirling flow impact on capsule-based DPI emptying was conducted using CFD. In this 194

Section, the simulation results will be demonstrated and then discussed from the physical point of view. The following results are presented for the last time-period (t = 0.2 s). The variations of ED with multiple airflow rates, d_{c_outlet}, and SPs are shown in Fig. 4. As can be seen, adding a small spiral vane (SP = 0.025) increases the percentage of ED for LPM = 3 and 4, whereas LPM = 4 has a more noticeable increase rate of ED. The ED percentages fall for larger SP. Additionally, Table 3 is presented to provide a quantitative perspective on the results presented in Fig. 4.

Figs. 5–7 display the effect of swirl parameters and outlet orifice diameter on velocity and turbulence kinetic energy for airflow rate equal to 4 LPM. The air jet formation, secondary flow, vorticities, and multiple recirculation zones are all visible (Figs. 5–7). In light of the physical point of view, a cross-section in the capsule containment was considered, and the velocity contours were plotted (Fig. 8). Fig. 9 demonstrates an overview of particle motion in a specific timestep for various values of SP. The particle's contour is determined by its velocity.

5. Discussion

The primary finding of the study is that the ED percent for LPM = 5 was found to decrease with even a small increase in SP, and generally, the ED percent for LPM = 5 drops rapidly as SP increases. Higher airflow rates also cause more ED, which is a common trend. However, this trend is not present in all SPs. Conversely, as SP increases, the ED percent dramatically declines. Moreover, it can be noticed when d_{c_outlet} become smaller, SP value falls. An elaborate discussion on all the above observations will be provided in the following.

As a second finding, with an elaborate probe at the contours, it can be inferred that the recirculation zones and their vorticities become more prominent and robust in the capsule section as d_{c_outlet} decreases. As a result, particles will become stuck in these zones, preventing dispersion. This results in a decrease in ED% as d_{c_outlet} increases. It can also be determined that the swirl parameter significantly impacts the flow

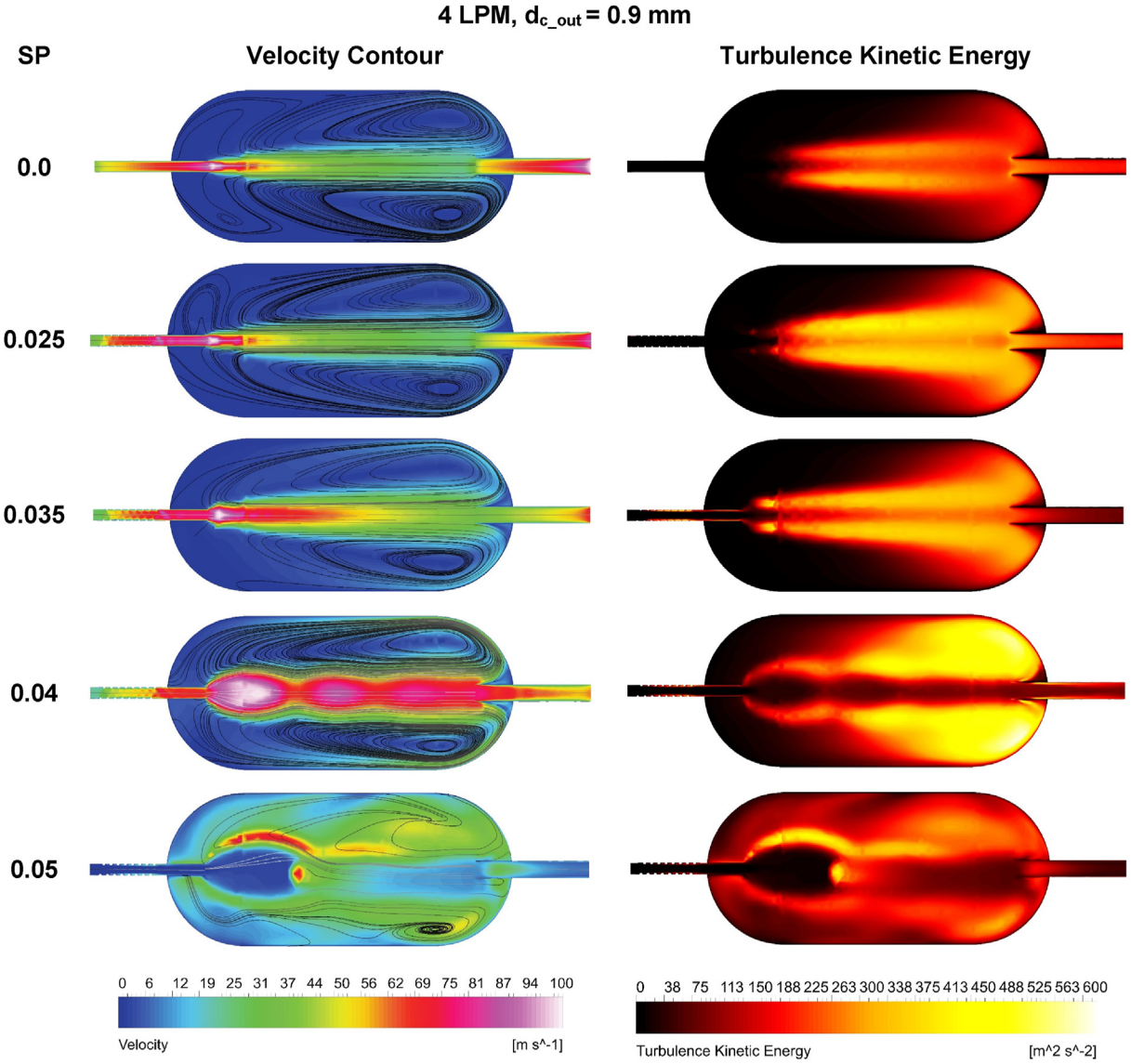

Fig. 6. Contour of velocity and turbulence kinetic energy of various SP for d_{c_out} = 0.9 mm and 4 LPM flow rate (t = 0.2 s).

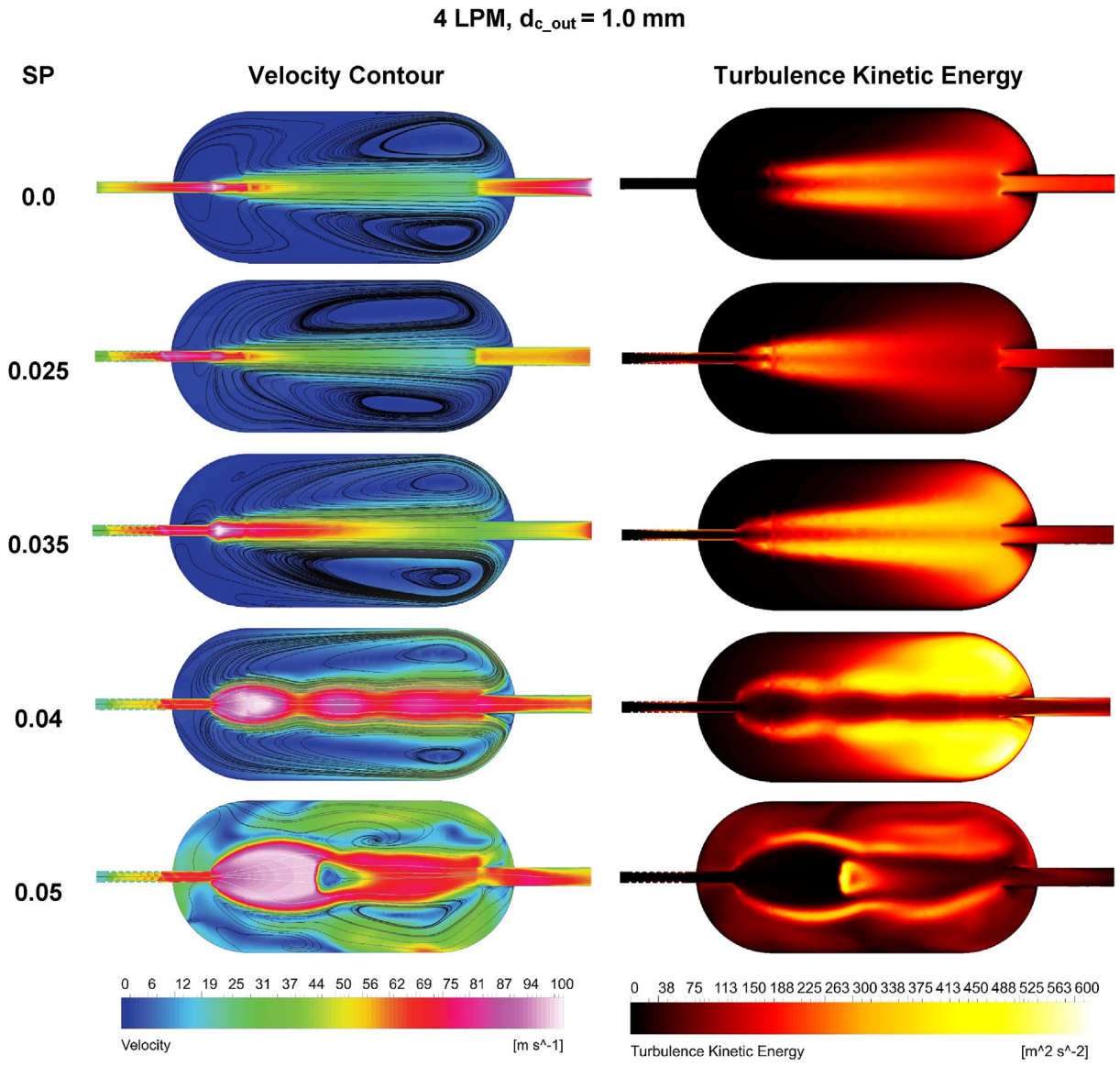

Fig. 7. Contour of velocity and turbulence kinetic energy of various SP for d_{c_out} = 1.0 mm and 4 LPM flow rate (t = 0.2 s).

pattern and turbulence kinetic energy. The recirculation zone expands slightly for smaller SPs and lower airflow rates, and the flow streamlines become more uniform and tighter. As a result of these positive effects, particles are properly dispersed, and the ED percent increases compared to no-swirl flow. However, the recirculation zones grow more extensive and robust as SP rises.

This causes more vortices to form in the capsule and near the outlet orifice, which is not perfect or favorable. Thus, particles cannot disperse well in the capsule and become trapped in these vorticities. Therefore, the ED % drops dramatically. This will occur with a low airflow rate and a high SP value.

In addition, no-swirl flow has symmetrical vorticities. For flow with SP = 0.025, this symmetry is also apparent. Due to this symmetry, centrifugal forces are generated in the cross-section's central zone, which increases the ED value. In contrast, symmetrical flows and vorticities disappeared for flows with higher SP values. The flow trend changed—the centrifugal force near the wall increased and moved toward the center. The flow becomes completely fluctuating at a high SP value, especially at a high airflow rate.

Besides, low SP allows particles to exit the capsule more effectively than no-swirl and higher-swirling flows. This illustration can support our previous discussion by describing particles' reactions to swirling flow.

6. Conclusion

In the present study, the authors focus on an inline capsule-based dry powder inhaler (DPI) and how to develop the design for effectively emptying the drug particles. Studying the impact of swirling flow on emptying the DPI was presented. To generate swirling flow, spiral vanes are placed on the inlet capillary (orifice). Different spiral depths (SD) are used, resulting in different swirl parameter values. The effect of outlet capillary diameter (d_{c_out}) and flow rates on emitted dose (ED) percentages is also explored.

The following conclusion can be drawn.

- At low airflow rates, swirling flow helps to better empty the capsule and increases ED by 5–20% when compared to no-swirl flow.

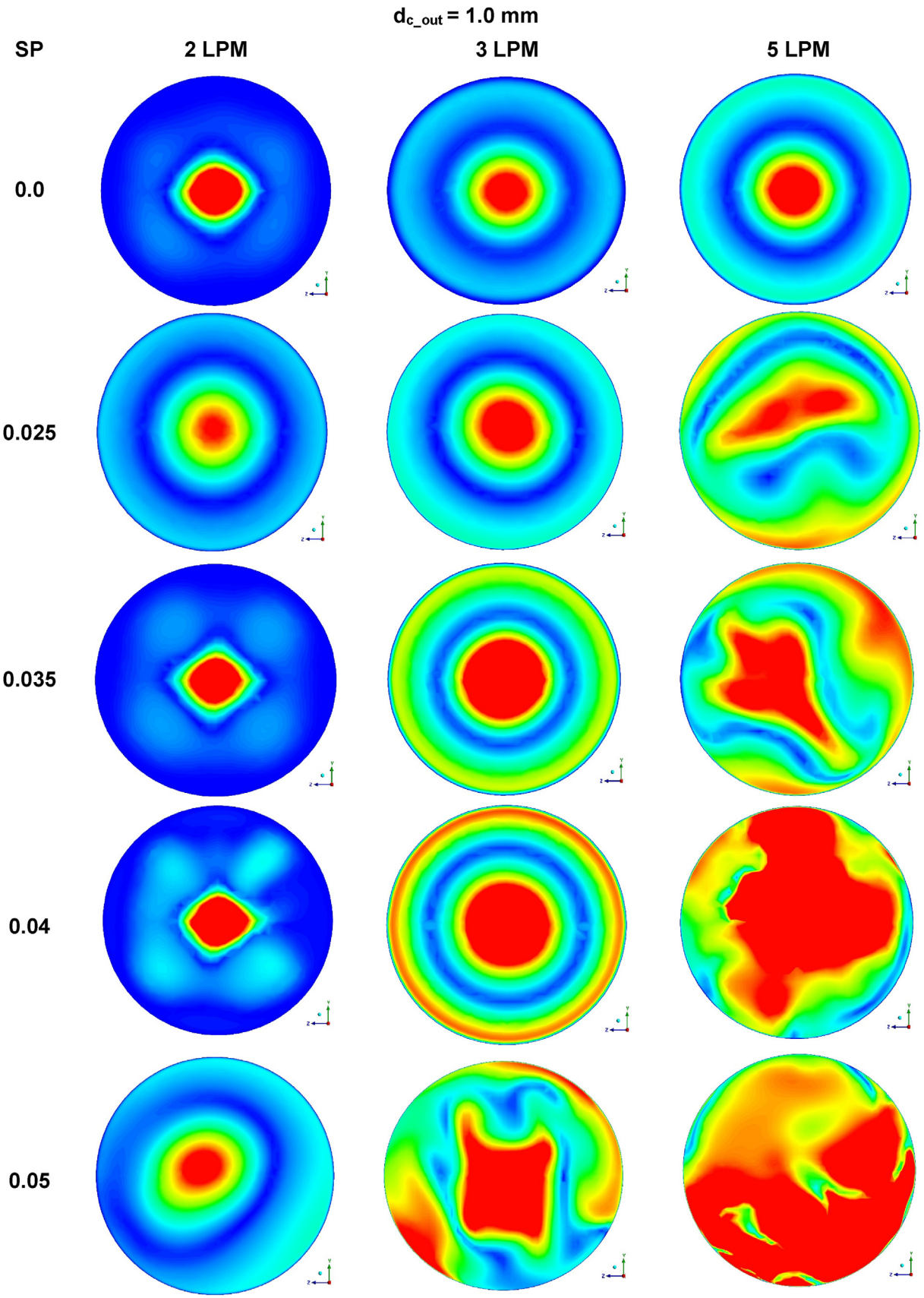

Fig. 8. Velocity contour pattern at a specified cross-section (middle of the capsule) of capsule for different SP and flow rate (t = 0.2 s).

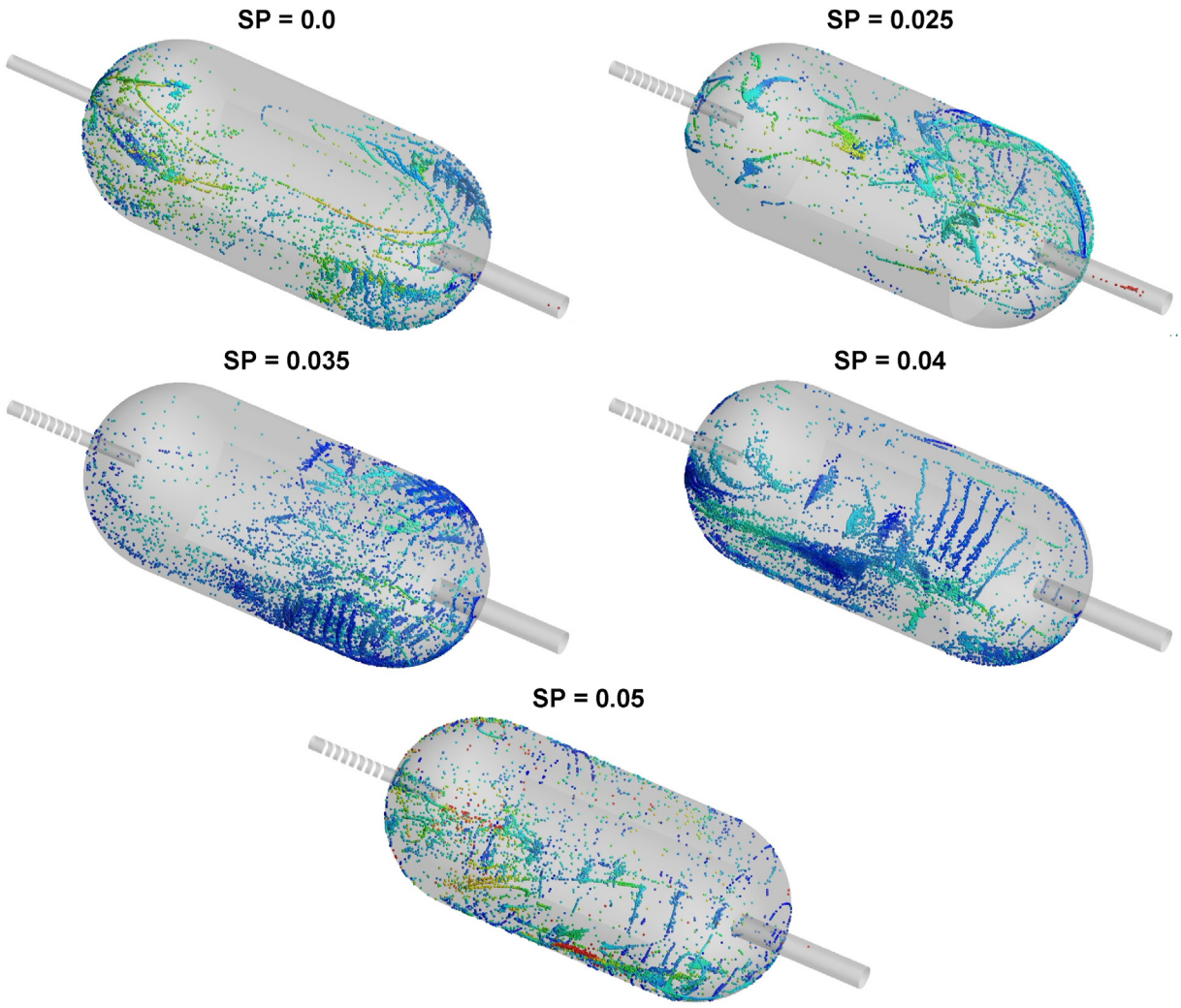

Fig. 9. Particle motion in a specific timestep (t = 0.01 s) for a flow rate of 3 LPM and d_{c_out} = 1.0 mm.

- Higher SP, on the other hand, has a negative effect and reduces the ED value by more than 50% due to the formation of vortices. The recirculation area, vorticities, and flow pattern all change as the flow rate and SP increase. As a result, the ED value falls noticeably.

Although the above results and conclusions apply only to the present study, this conclusion provides insight into future device designs.

Funding resource

This work was supported the National Natural Science Foundation of China (grant No.12172146).

Author contribution

Mohammad Hasan Taheri: Investigation; Methodology; Validation; Roles/Writing - original draft; Writing - review & editing, Nematollah Askari: Software; Writing - review & editing, Yaning Feng: Writing - review & editing, Malikeh Nabaei: Writing - review & editing, Mohammad S. Islam: Writing - review & editing, Ali Farnoud: Writing - review & editing, Xinguang Cui: Conceptualization; Funding acquisition; Investigation; Methodology; Supervision; Roles/Writing - original draft; Writing - review & editing.

Declaration of competing interest

I wish to confirm that there are no known conflicts of interest associated with this publication and there has been no significant financial support for this work that could have influenced its outcome. I confirm that the manuscript has been read and approved by all named authors and that there are no other persons who satisfied the criteria for authorship but are not listed. I further confirm that the order of authors listed in the manuscript has been approved by all of us.

I understand that the corresponding author is the sole contact for the Editorial process (including Editorial Manager and direct communications with the office). Corresponding authoe is responsible for communicating with the other authors about progress, submissions of revisions and final approval of proofs. I confirm that I have provided a current, correct email address which is accessible by the corresponding author and which has been configured to accept email from (xinguang_cui@hust.edu.cn).

References

[1] Dal Negro RW. Dry powder inhalers and the right things to remember: a concept review. Multidis Res Med 2015;10(1):1–4. https://doi.org/10.1186/s40248-015-0012-5.

[2] Kou X, Heng PW, Chan LW, Wereley ST, Carvajal MT. Effect of roughness on the dispersion of dry powders for inhalation: a dynamic visualization perspective. AAPS PharmSciTech 2019;20(7):1–11. https://doi.org/10.1208/s12249-019-1482-0.

[3] de Boer AH, Hagedoorn P, Hoppentocht M, Buttini F, Grasmeijer F, Frijlink HW. Dry powder inhalation: past, present and future. Expet Opin Drug Deliv 2017;14(4):499–512. https://doi.org/10.1080/17425247.2016.1224846.
[4] Suwandecha T, Wongpoowarak W, Srichana T. Computer-aided design of dry powder inhalers using computational fluid dynamics to assess performance. Pharmaceut Dev Technol 2016;21(1):54–60. https://doi.org/10.3109/10837450.2014.965325.
[5] Lavorini F, Pistolesi M, Usmani OS. Recent advances in capsule-based dry powder inhaler technology. Multidis Res Med 2017;12(1):1–7. https://doi.org/10.1186/s40248-017-0092-5.
[6] Coates MS, Chan H-K, Fletcher DF, Raper JA. Effect of design on the performance of a dry powder inhaler using computational fluid dynamics. Part 2: air inlet size. J Pharmaceut Sci 2006;95(6):1382–92. https://doi.org/10.1002/jps.20603.
[7] Ke WR, Chang RYK, Kwok PCL, Tang P, Chen L, Chen D, et al. Administration of dry powders during respiratory supports. Ann Transl Med 2021;9(7):596. https://doi.org/10.21037/atm-20-3946.
[8] Howe C, Hindle M, Bonasera S, Rani V, Longest PW. Initial development of an air-jet dry powder inhaler for rapid delivery of pharmaceutical aerosols to infants. J Aerosol Med Pulm Drug Deliv 2020;34(1):57–70. https://doi.org/10.1089/jamp.2020.1604.
[9] Ahookhosh K, Yaqoubi S, Mohammadpourfard M, Hamishehkar H, Aminfar H. Experimental investigation of aerosol deposition through a realistic respiratory airway replica: an evaluation for MDI and DPI performance. Int J Pharm 2019;566:157–72. https://doi.org/10.1016/j.ijpharm.2019.05.058.
[10] Hoppentocht M, Hoste C, Hagedoorn P, Frijlink HW, de Boer AH. In vitro evaluation of the DP-4M PennCentury™ insufflator. Eur J Pharm Biopharm 2014;88(1):153–9. https://doi.org/10.1016/j.ejpb.2014.06.014.
[11] Laube BL, Sharpless G, Shermer C, Sullivan V, Powell K. Deposition of dry powder generated by solovent in Sophia Anatomical infant nose-throat (SAINT) model. Aerosol Sci Technol 2012;46(5):514–20. https://doi.org/10.1080/02786826.2011.643257.
[12] Duret C, Wauthoz N, Merlos R, Goole J, Maris C, Roland I, et al. In vitro and in vivo evaluation of a dry powder endotracheal insufflator device for use in dose-dependent preclinical studies in mice. Eur J Pharm Biopharm 2012;81(3):627–34. https://doi.org/10.1016/j.ejpb.2012.04.004.
[13] Morello M, Krone CL, Dickerson S, Howerth E, Germishuizen WA, Wong Y-L, et al. Dry-powder pulmonary insufflation in the mouse for application to vaccine or drug studies. TB 2009;89(5):371–7. https://doi.org/10.1016/j.tube.2009.07.001.
[14] Bass K, Farkas D, Hassan A, Bonasera S, Hindle M, Longest PW. High-efficiency dry powder aerosol delivery to children: review and application of new technologies. J. Aerosol. Sci 2021;153:105692. https://doi.org/10.1016/j.jaerosci.2020.105692.
[15] Farkas D, Hindle M, Bonasera S, Bass K, Longest W. Development of an inline dry powder inhaler for oral or trans-nasal aerosol administration to children. J Aerosol. Med. Pulm. Drug. Deliv. 2020;33(2):83–98. https://doi.org/10.1089/jamp.2019.1540.
[16] Farkas D, Bonasera S, Bass K, Hindle M, Longest PW. Advancement of a positive-pressure dry powder inhaler for children: use of a vertical aerosolization chamber and three-dimensional rod array interface. Pharm. Res. (N Y) 2020;37(9):1–14. https://doi.org/10.1007/s11095-020-02889-7.
[17] Longest W, Farkas D, Bass K, Hindle M. Use of computational fluid dynamics (CFD) dispersion parameters in the development of a new DPI actuated with low air volumes. Pharm. Res. (N Y) 2019;36(8):1–17. https://doi.org/10.1007/s11095-019-2644-1.
[18] Longest W, Farkas D. Development of a new inhaler for high-efficiency dispersion of spray-dried powders using computational fluid dynamics (CFD) modeling. AAPS J. 2019;21(2):1–15. https://doi.org/10.1208/s12248-018-0281-y.
[19] Bass K, Farkas D, Longest W. Optimizing aerosolization using computational fluid dynamics in a pediatric air-jet dry powder inhaler. AAPS Pharm. Sci. Tech 2019;20(8):329. https://doi.org/10.1208/s12249-019-1535-4.
[20] Bass K, Farkas D, Longest W. Optimizing aerosolization using computational fluid dynamics in a pediatric air-jet dry powder inhaler. AAPS Pharm. Sci. Tech. 2019;20(8):1–19. https://doi.org/10.1208/s12249-019-1535-4.
[21] Longest PW, Hindle M, Son Y-J, Behara SRB, Farkas D. Dry powder inhaler (DPI) designs for producing aerosols with high fine particle fractions. Google Patents; 2018.
[22] Farkas D, Hindle M, Longest PW. Development of an inline dry powder inhaler that requires low air volume. J Aerosol Med Pulm Drug Deliv 2018;31(4):255–65. 10.1089%2Fjamp.2017.1424.
[23] Farkas D, Hindle M, Longest P. Development of a high efficiency inline dry powder inhaler that requires low air volume. J Aerosol Med Pulm Drug Deliv. 30. New Rochelle, NY 10801 USA: Mary Ann Liebert, INC 140 Huguenot Street, 3RD FL; 2017. p. 22.
[24] Farkas DR, Hindle M, Longest PW. Characterization of a new high-dose dry powder inhaler (DPI) based on a fluidized bed design. Ann. Biomed. Eng 2015;43(11):2804–15. https://doi.org/10.1007/s10439-015-1335-2.
[25] Ahookhosh K, Saidi M, Aminfar H, Mohammadpourfard M, Hamishehkar H, Yaqoubi S. Dry powder inhaler aerosol deposition in a model of tracheobronchial airways: validating CFD predictions with in vitro data. Int. J. Pharm 2020;587:119599. https://doi.org/10.1016/j.ijpharm.2020.119599.
[26] Ahookhosh K, Saidi M, Mohammadpourfard M, Aminfar H, Hamishehkar H, Farnoud A, et al. Flow structure and particle deposition analyses for optimization of a pressurized metered dose inhaler (pMDI) in a model of tracheobronchial airway. Eur. J. Pharmaceut Sci. 2021;164:105911. https://doi.org/10.1016/j.ejps.2021.105911.
[27] Dai W, Huang F, Yu J, Li R, Tong Z. Numerical study of effects of device design on drug delivery efficiency for an active dry powder inhaler. J. Aerosol Sci 2021;157:105801. https://doi.org/10.1016/j.jaerosci.2021.105801.
[28] Gurumurthy A, Kleinstreuer C. Analysis of improved oral drug delivery with different helical stream inhalation modes. Comput. Biol. Med. 2022;141:105132. https://doi.org/10.1016/j.compbiomed.2021.105132.
[29] Last TS, Stemme G, Roxhed N. First micro swirl nozzle for fast drug delivery to the lung. In: IEEE 34th International Conference on Micro Electro Mechanical Systems (MEMS); 2021. p. 22–5. 2021.
[30] Alfano FO, Di Maio FP, Di Renzo A. Deagglomeration of selected high-load API-carrier particles in swirl-based dry powder inhalers. Powder Technol 2022;408:117800. https://doi.org/10.1016/j.powtec.2022.117800.
[31] Sommerfeld M. Detailed evaluation of drug powder deposition in swirl-type dry powder inhalers. Powder Technol. 2022;407:117687. https://doi.org/10.1016/j.powtec.2022.117687.
[32] Arsalanloo A, Abbasalizadeh M. Numerical study on deposition of particles in a 90° bend in the presence of swirling flow using Eulerian-Lagrangian method. Powder Technol 2017;320:285–94. https://doi.org/10.1016/j.powtec.2017.07.050.
[33] Bass K, Longest PW. Recommendations for simulating microparticle deposition at conditions similar to the upper airways with two-equation turbulence models. J Aerosol Sci 2018;119:31–50. https://doi.org/10.1016/j.jaerosci.2018.02.007.
[34] Moskal A, Sosnowski TR. Computational fluid dynamics (CFD) and direct visualization studies of aerosol release from two cyclohaler-type dry powder inhalers. J. Drug. Deliv. Sci. Technol. 2012;22(2):161–5. https://doi.org/10.1016/S1773-2247(12)50021-3.
[35] Longest PW, Hindle M, Choudhuri SD, Byron PR. Numerical simulations of capillary aerosol generation: CFD model development and comparisons with experimental data. Aerosol. Sci. Technol. 2007;41(10):952–73. https://doi.org/10.1080/02786820701607027.
[36] Wilcox DC. Turbulence modeling for CFD. second ed. CA: DCW industries La Canada; 1998.
[37] Rahimi-Gorji M, Gorji TB, Gorji-Bandpy M. Details of regional particle deposition and airflow structures in a realistic model of human tracheobronchial airways: two-phase flow simulation. Comput. Biol. Med. 2016;74:1–17. https://doi.org/10.1016/j.compbiomed.2016.04.017.
[38] Pourmehran O, Gorji TB, Gorji-Bandpy M. Magnetic drug targeting through a realistic model of human tracheobronchial airways using computational fluid and particle dynamics. Biomech. Model Mechanobiol 2016;15(5):1355–74. https://doi.org/10.1007/s10237-016-0768-3.